PROCEEDINGS OF SCIENCE

Magnetic polarizability of a charged pion from four-point functions

Frank Lee,[a,*] **Walter Wilcox,**[b] **Andrei Alexandru**[a] **and Chris Culver**[c]

[a] *Physics Department, The George Washington University, Washington, DC 20052, USA*
[b] *Department of Physics, Baylor University, Waco, Texas 76798, USA*
[c] *Department of Mathematical Sciences, University of Liverpool, Liverpool L69 7ZL, United Kingdom*

E-mail: fxlee@gwu.edu, walter_wilcox@baylor.edu

Electromagnetic dipole polarizabilities are fundamental properties of a hadron that represent its resistance to deformation under external fields. For a charged hadron, the presence of acceleration and Landau levels complicates the isolation of its deformation energy in the conventional background field method. In this work, we explore a general method based on four-point functions in lattice QCD that takes into account all photon, quark and gluon interactions. The electric polarizability (α_E) has been determined from the method in a previous proof-of-principle simulation. Here we focus on the magnetic polarizability (β_M) using the same quenched Wilson action on a $24^3 \times 48$ lattice at $\beta = 6.0$ with pion mass from 1100 to 370 MeV. The results from the connected diagrams show a large cancellation between the elastic and inelastic contributions, leading to a relatively small and negative value for β_M consistent with chiral perturbation theory.

The 40th International Symposium on Lattice Field Theory (Lattice 2023)
July 31st - August 4th, 2023
Fermi National Accelerator Laboratory

*Speaker

PoS(LATTICE2023)303

1. Introduction

Understanding electromagnetic polarizabilities has been a long-term goal of lattice QCD. The standard approach is the background field method which introduces classical static electromagnetic fields to interact with quarks in QCD.The appeal of the method lies in its simplicity: only two-point correlation functions are needed to measure the small energy shift with or without the external field, which amounts to a standard calculation of a hadron's mass. The energy shift linear in the applied field is related to dipole moments, and the quadratic shift to polarizabilities. The method is fairly robust and has been widely applied to neutral hadrons.

When it comes to charged hadrons, however, the method is faced with new challenges. The reason is rather rudimentary: a charged particle accelerates in an electric field and exhibits Landau levels in a magnetic field. Such collective motion of the hadron is unrelated to moments and polarizabilities and must be disentangled from the total energy shift in order to isolate the deformation energy on which the polarizabilities are defined. The traditional method of extracting ground state energy at large times breaks down since the two-point function no longer has a single-exponential behavior. Special techniques have to be developed to analyze such functions.

Here we advocate an alternative approach based on four-point functions in lattice QCD. Instead of background fields, electromagnetic currents couple to quark fields. All photon-quark, quark-quark, and gluon-quark interactions are included. It is a general approach that treats neutral and charged particles on equal footing. The potential of using four-point functions to access polarizabilities has been investigated in the early days of lattice QCD [1–3]. The effort was deemed too computationally demanding at the time and the results on limited lattices were inconclusive. Recently, there is a renewed interest to revive such efforts, partly spurred by the challenges encountered in the background field method for charged particles. A reexamination of the formalism in Ref. [3] is carried out in Ref. [4] in which new formulas are derived in momentum space for electric and magnetic polarizabilities of both charged pion and proton. It is followed by a proof-of-principle simulation for the electric polarizability of a charged pion [5]. In this work, we extend the calculation to magnetic polarizability using the same lattice parameters. We note there exists other four-point function calculations on polarizabilities. Ref.[6] employs a position-space formula for the Compton tensor to calculate charge pion electric polarizability near the physical point, along with a calculation on the proton [7]. A comprehensive review on pion polarizabilities from other theoretical approaches and experiment can be found in Ref. [8, 9]. We also note that although Refs. [10, 11] are based on the background field method, they are in fact four-point function calculations.

2. Methodology

In Ref. [4], a formula is derived for electric polarizability of a charged pion,

$$\alpha_E = \frac{\alpha\langle r_E^2\rangle}{3m_\pi} + \lim_{\boldsymbol{q}\to 0}\frac{2\alpha}{\boldsymbol{q}^2}\int_0^\infty dt\Big[Q_{44}(\boldsymbol{q},t) - Q_{44}^{elas}(\boldsymbol{q},t)\Big], \tag{1}$$

and for its magnetic polarizability,

$$\beta_M = -\frac{\alpha\langle r_E^2\rangle}{3m_\pi} + \lim_{\boldsymbol{q}\to 0}\frac{2\alpha}{\boldsymbol{q}^2}\int_0^\infty dt\Big[Q_{11}^{inel}(\boldsymbol{q},t) - Q_{11}^{inel}(\boldsymbol{0},t)\Big]. \tag{2}$$

Here $\alpha = 1/137$ is the fine structure constant.

The formulas are in discrete Euclidean spacetime but we keep the time axis continuous for notational convenience. Zero-momentum Breit frame is employed in the formula to mimic low-energy Compton scattering, where the initial and final pions are at rest and the photons have purely spacelike momentum. The formulas have a similar structure in that they both have an elastic contribution in terms of the charge radius and pion mass, and an inelastic contribution in the form of subtracted time integrals. They differ in two aspects. The Q_{44} in α_E includes both elastic and inelastic contributions whereas the Q_{11}^{inel} in β_M includes only inelastic contributions. In α_E, the elastic $Q_{44}^{elas}(\boldsymbol{q}, t)$ is subtracted, whereas in β_M it is the zero-momentum inelastic $Q_{11}^{inel}(\boldsymbol{0}, t)$ that is subtracted.

Both α_E and β_M have the expected physical unit of a^3 (fm^3). In the elastic term $\langle r_E^2 \rangle$ scales like a^2 and m_π like a^{-1}. In the inelastic term $1/\boldsymbol{q}^2$ scales like a^2, t scales like a, and Q_{44} and Q_{11} are dimensionless by definition. The α_E has been studied thoroughly in a previous work [5], from which we take the results for pion mass m_π and charge radius $\langle r_E^2 \rangle$ and α_E. In this work we focus on the β_M in Eq. (2).

The four-point function Q_{11} is defined as,

$$Q_{11}(\boldsymbol{q}, t_3, t_2, t_1, t_0) \equiv \frac{\sum_{\boldsymbol{x}_3, \boldsymbol{x}_2, \boldsymbol{x}_1, \boldsymbol{x}_0} e^{-i\boldsymbol{q}\cdot\boldsymbol{x}_2} e^{i\boldsymbol{q}\cdot\boldsymbol{x}_1} \langle \Omega | \psi(x_3) : j_1^L(x_2) j_1^L(x_1) : \psi^\dagger(x_0) | \Omega \rangle}{\sum_{\boldsymbol{x}_3, \boldsymbol{x}_0} \langle \Omega | \psi(x_3) \psi^\dagger(x_0) | \Omega \rangle}. \tag{3}$$

Wick contractions of quark-antiquark pairs in the unsubtracted part lead to topologically distinct quark-line diagrams shown in Fig. 1. The total connected contribution is simply the sum of the

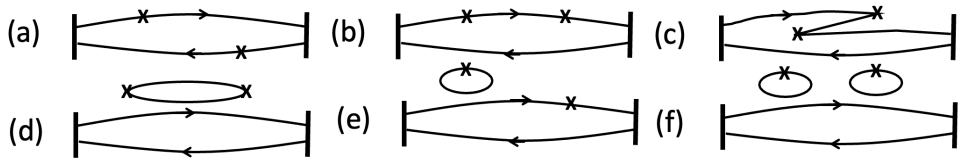

Figure 1: Quark-line diagrams of a four-point function contributing to polarizabilities of a meson. connected insertions (a), (b), (c); and disconnected insertions (d), (e), (f). The zero-momentum pion interpolating fields are represented by vertical bars (wall sources).

individual normalized terms,

$$Q_{11}(\boldsymbol{q}, t_2, t_1) = Q_{11}^{(a)} + Q_{11}^{(b)} + Q_{11}^{(c)}. \tag{4}$$

The charge factors and flavor-equivalent contributions have been included in each diagram.

3. Simulation details and results

We use quenched Wilson action with $\beta = 6.0$ and $\kappa = 0.1520,\ 0.1543,\ 0.1555,\ 0.1565$ on the lattice $24^3 \times 48$. We analyzed 500 configurations for $\kappa = 0.1520$ and 1000 configurations each for rest of the kappas. The scale of this action is set with inverse lattice spacing $1/a = 2.312$ GeV and kappa critical $\kappa_c = 0.15708$. Dirichlet (or open) boundary condition is imposed in the time direction, while periodic boundary conditions are used in spatial dimensions. The pion source

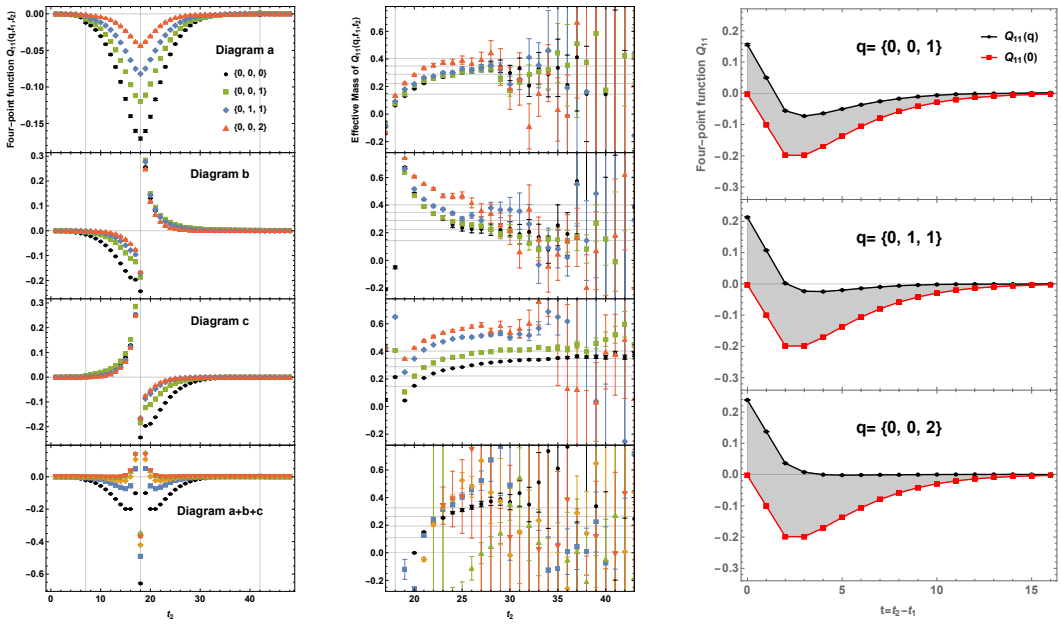

Figure 2: Individual and total four-point functions (left), their effective mass functions (middle), and isolated signal for Q_{11} from the connected diagrams as a function of current separation at $m_\pi = 600$ MeV. The shaded area between the two is the dimensionless signal contributing to magnetic polarizability. Horizontal gridlines in the effective mass functions are $E_\rho - m_\pi$ in lattice units where $E_\rho = \sqrt{\boldsymbol{q}^2 + m_\rho^2}$ with measured m_π and m_ρ.

is placed at $t_0 = 7$ and sink at $t_3 = 42$ (time is labeled from 1 to 48). One current is inserted at a fixed time t_1, while the other current t_2 is free to vary. We consider four different combinations of momentum $\boldsymbol{q} = \{0,0,0\}$, $\{0,0,1\}$, $\{0,1,1\}$, $\{0,0,2\}$. In lattice units they correspond to the values $\boldsymbol{q}^2a^2 = 0,\ 0.068,\ 0.137,\ 0.274$, or in physical units to $\boldsymbol{q}^2 = 0,\ 0.366,\ 0.733,\ 1.465$ (GeV^2).

In Fig. 2 we show the raw normalized four-point functions, both individually and collectively, at the four different values of momentum $\boldsymbol{q}$ and at $m_\pi = 600$ MeV. All points are included and displayed on a linear scale for comparison purposes. The special point of $t_1 = t_2$ is regular in diagram a, but gives irregular results in diagram b and c at all values of $\boldsymbol{q}$. The same irregularity is observed in the electric case. It is an unphysical contact interaction on the lattice which vanishes in the continuum limit. We treat this point with special care in our analysis below. The results about $t_1 = 18$ in diagram b and c are mirror images of each other, simply due to the fact that they are from the two different time orderings of the same diagram. In principle, this property could be exploited to reduce the cost of simulations by placing t_1 in the center of the lattice. In this study, however, we computed all three diagrams separately, and add them between $t_1 = 19$ and $t_3 = 41$ as the signal. There is no elastic contribution in the second term of β_M in Eq.(2) as long as transverse momentum to j_1^L is considered. This is evident in the effective mass functions in Fig. 2 where the intermediate states are not on-shell pions, but states with different mass and energy. Possible intermediate states are either vector or axial mesons in the magnetic channel. For reference, we draw horizontal lines $E_\rho - m_\pi$ in lattice units where $E_\rho = \sqrt{\boldsymbol{q}^2 + m_\rho^2}$, using measured m_π and m_ρ. The effective mass functions in Fig. 2 are

only provided for reference purposes on the intermediate state. They can become noisy at large current separations and higher momentum. This is not a concern since there is no fitting performed at large times. The signal is the time integral of subtracted four-point functions, which amounts to evaluating the area between two curves. And the signal is dominant at small times.

In the right panel of Fig. 2 we show the connected contribution $Q_{11}(\boldsymbol{q})$ at different $\boldsymbol{q}$ values and zero-momentum $Q_{11}(\boldsymbol{0})$ as a function of current separation $t = t_2 - t_1$ in lattice units. Only results for $m_\pi = 600$ MeV are shown as an example; the graphs at the other pion masses look similar. The time integral required for β_M in the formula, $(1/a)\int dt\big[Q_{11}(\boldsymbol{q},t) - Q_{11}(\boldsymbol{0},t)\big]$, is simply the shaded area between the two curves, and it is positive. One detail to notice is that the curves include the $t = 0$ point which has unphysical contributions in Q_{11} mentioned earlier. We would normally avoid this point and only start the integral from $t = 1$. However, the chunk of area between $t = 0$ and $t = 1$ is the largest piece in the integral. To include this contribution, we linearly extrapolated both $Q_{11}(\boldsymbol{q})$ and $Q_{11}(\boldsymbol{0})$ back to $t = 0$ using the two points at $t = 1$ and $t = 2$. As the continuum limit is approached, the $t = 0$ point will become regular and the chunk will shrink to zero.

The inelastic term can now be constructed by multiplying $2\alpha/\boldsymbol{q}^2$ and the time integral, and it is a function of momentum. Since β_M is a static property, we extrapolate it to $\boldsymbol{q}^2 = 0$ smoothly. We consider two fits, a quadratic fit $a + b\,x + c\,x^2$ ($x = \boldsymbol{q}^2$) using all three data points, and a linear fit using the two lowest points. The results are shown in Fig. 3 for all pion masses. One observes a spread in the extrapolated values at $\boldsymbol{q}^2 = 0$. We treat the spread as a systematic effect as follows. We take the average of the two extrapolated values along with statistical uncertainties, and half of the difference in their central values as a systematic uncertainty. The statistical and systematic uncertainties are then propagated in quadrature to the analysis of β_M. For our data, the statistical uncertainties are relatively small, so the systematic uncertainties are dominant in the inelastic contribution.

Finally, we assemble the two terms in the formula in Eq.(2) to obtain β_M in physical units. At each pion mass the elastic term is negative, whereas the inelastic term is positive. The total is slightly positive at the two heaviest pion masses, then turns negative as the pion mass is lowered. To see how the trend continues to smaller pion masses, we take the total values for β_M at the four pion masses

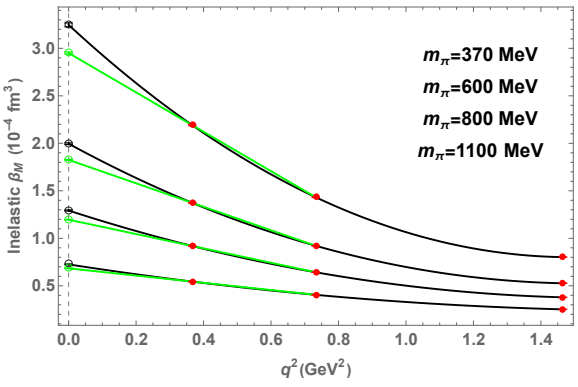

Figure 3: Momentum dependence of the inelastic term in Eq. (2) and its extrapolation to $\boldsymbol{q}^2 = 0$ at all pion masses. Red points are based on the shaded areas in Fig. 2. Black curve is a quadratic extrapolation using all three points. Green curve is a linear extrapolation based on the two lowest points. Empty points indicate the corresponding extrapolated values contributing to β_M.

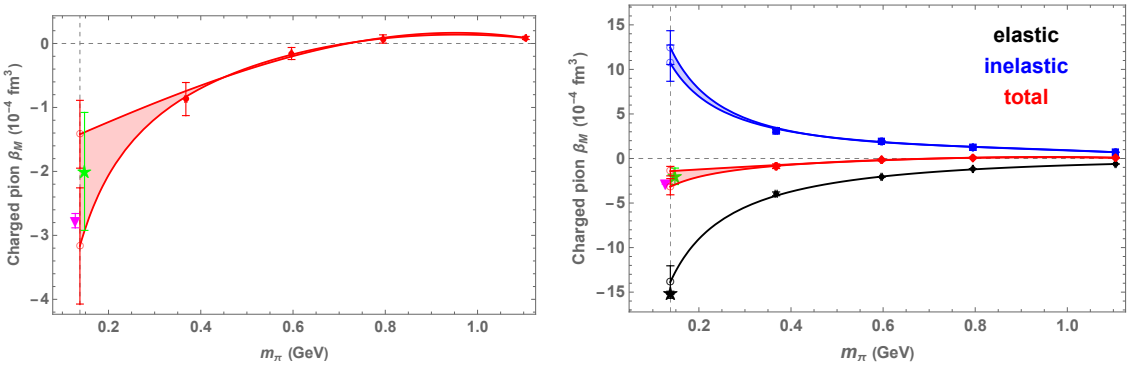

Figure 4: Left: chiral extrapolation of charged pion magnetic polarizability. Right: individual and total contributions to charged pion β_M (right) from four-point functions in lattice QCD based on the formula in Eq.(2). The total is taken from the left, and the elastic from Ref. [5]; both are chirally extrapolated to the physical point. The inelastic is from the difference of the two.

and perform a smooth extrapolation to the physical point. Since our pion passes are relatively large, we consider two forms to cover the range of uncertainties in the extrapolation: a polynomial form $a + b\,m_\pi + c\,m_\pi^3$ and a form with a divergent $1/m_\pi$ term $\frac{a}{m_\pi} + b\,m_\pi + c\,m_\pi^3$ inspired by ChPT [12]. The spread can be considered as a systematic effect. The extrapolated value of -3.2 ± 0.9 to -1.4 ± 0.5 at the physical point is comparable to the known value of $-2.0 \pm 0.6 \pm 0.7$ from PDG and $-2.77(11)$ from two-loop contribution of ChPT [9, 12]. An interesting feature is a sign change from positive to negative as pion mass is lowered. It happens around 750 MeV. In contrast, there is no sign change in the electric case.

A comparison on β_M can be made here between the four-point function method and the background field method. For the former, our value of $-3.2(9)$ is the only attempt at the moment. For the latter, there are several calculations. In Ref. [13, 14], β_M is studied for both charged and neutral pions. A fitting form is used that includes Landau levels and up to B^4 contributions in magnetic field for charged pions. Values of $-1.15(31)$ and $-2.06(76)$ are obtained on two different lattices. No chiral extrapolation is performed. Since only bare quark masses are given we could not ascertain what pion masses they correspond to. In Ref. [15], a Laplacian-mode projection technique is employed at the quark propagator level to filter out the Landau levels. The same technique is used on the nucleon [16]. A final value of $-1.70(14)(25)$ is reported. It also predicts a sign change in β_M, but only after chiral extrapolation. The simulated results are positive at all the pion masses considered, down to about 300 MeV. A Padé form is introduced to extrapolate the positive values to the negative one at the physical point. The sign change happens at around 225 MeV. This is different from the sign change observed in Fig. 4, which happens at a heavier pion mass, before chiral extrapolation. This is an interesting puzzle for future investigations. The resolution could be in the different systematics present in the two calculations. For the four-point function method in this work, it could be the quenched approximation, disconnected diagrams, and the contact term in the connected diagrams.

This work was supported in part by U.S. Department of Energy under Grant No. DE-FG02-95ER40907 (FL, AA) and UK Research and Innovation grant MR/S015418/1 (CC). WW would like to acknowledge support from the Baylor College of Arts and Sciences SRA program. AA

would like to acknowledge support from University of Maryland. The calculations are carried out at DOE-sponsored NERSC at Livermore and NSF-sponsored TACC at Austin.

References

[1] M. Burkardt, J. Grandy and J. Negele, *Calculation and interpretation of hadron correlation functions in lattice qcd*, *Annals of Physics* **238** (1995) 441.

[2] W. Andersen and W. Wilcox, *Lattice charge overlap. 1. Elastic limit of pi and rho mesons*, *Annals Phys.* **255** (1997) 34 [hep-lat/9502015].

[3] W. Wilcox, *Lattice charge overlap. 2: Aspects of charged pion polarizability*, *Annals Phys.* **255** (1997) 60 [hep-lat/9606019].

[4] W. Wilcox and F.X. Lee, *Towards charged hadron polarizabilities from four-point functions in lattice QCD*, *Phys. Rev. D* **104** (2021) 034506 [2106.02557].

[5] F.X. Lee, A. Alexandru, C. Culver and W. Wilcox, *Charged pion electric polarizability from four-point functions in lattice QCD*, *Phys. Rev. D* **108** (2023) 014512 [2301.05200].

[6] X. Feng, T. Izubuchi, L. Jin and M. Golterman, *Pion electric polarizabilities from lattice QCD*, *PoS* **LATTICE2021** (2022) 362 [2201.01396].

[7] X.-H. Wang, C.-L. Fan, X. Feng, L.-C. Jin and Z.-L. Zhang, *Nucleon electric polarizabilities and nucleon-pion scattering at physical pion mass*, 2310.01168.

[8] M. Moinester, *Pion Polarizability 2022 Status Report*, 5, 2022 [2205.09954].

[9] M. Moinester and S. Scherer, *Compton Scattering off Pions and Electromagnetic Polarizabilities*, *Int. J. Mod. Phys. A* **34** (2019) 1930008 [1905.05640].

[10] M. Engelhardt, *Neutron electric polarizability from unquenched lattice QCD using the background field approach*, *Phys. Rev. D* **76** (2007) 114502 [0706.3919].

[11] M. Engelhardt, *Exploration of the electric spin polarizability of the neutron in lattice QCD*, *PoS* **LATTICE2011** (2011) 153 [1111.3686].

[12] J. Gasser, M. Ivanov and M. Sainio, *Revisiting gamma + gamma to pi+ and pi- at low energies*, *Nuclear Physics B* **745** (2006) 84.

[13] E. Luschevskaya, O. Solovjeva, O. Kochetkov and O. Teryaev, *Magnetic polarizabilities of light mesons in su(3) lattice gauge theory*, *Nuclear Physics B* **898** (2015) 627.

[14] E.V. Luschevskaya, O.E. Solovjeva and O.V. Teryaev, *Magnetic polarizability of pion*, *Phys. Lett. B* **761** (2016) 393 [1511.09316].

[15] F. He, D.B. Leinweber, A.W. Thomas and P. Wang, *Chiral extrapolation of the charged-pion magnetic polarizability with Padé approximant*, 2104.09963.

[16] R. Bignell, W. Kamleh and D. Leinweber, *Magnetic polarizability of the nucleon using a Laplacian mode projection*, *Phys. Rev. D* **101** (2020) 094502 [2002.07915].